ELSEVIER

Physica D 117 (1998) 77–94

PHYSICA D

Symbolic dynamics behind the singular continuous power spectra of continuous flows

Michael A. Zaks *, Arkady S. Pikovsky, Jürgen Kurths

Department of Physics, Potsdam University, Postfach 601553, D-14415 Potsdam, Germany

Received 12 June 1997; received in revised form 21 November 1997; accepted 19 December 1997
Communicated by H. Müller-Krumbhaar

Abstract

We investigate a class of dissipative flows which possess singular continuous (fractal) power spectra. The attractor for these flows contains a saddle point, so that the times between the returns of an orbit onto a secant plane are unbounded. As a result, the Poincaré map does not reflect precisely the qualitative dynamics of the underlying flow: the power spectrum of this map can be discrete. We introduce the construction which takes into account that the time intervals between the intersections of the Poincaré plane can vary and construct a symbolic representation for the continuous process with logarithmic divergence in the distribution of such intervals. Spectral properties of the resulting symbolic sequences are shown to reproduce rather well those of the original flow. Copyright © 1998 Elsevier Science B.V.

PACS: 05.45+b; 02.30.Nw
Keywords: Return mappings; Singular continuous spectra; Multifractality

1. Introduction

The common way to obtain the discretized description of a continuous process is to mimic the flow by some recurrent relation binding the current position of the imaging point to its location at certain future and/or past moments. This construction replaces the continuous independent variable by an integer. A remarkably efficient tool for this is the Poincaré map which interrelates two consecutive returns onto some appropriate part of a suitably chosen codimension-1 surface (Poincaré surface) in the phase space; it is required that the relevant orbits intersect this surface transversely. In many situations the dynamics of the flow is adequately reproduced by the dynamics of the Poincaré map. Accordingly, there is a widespread feeling that the reduction to the map is an innocent procedure which preserves the dynamical features completely. However, this is not necessarily the case, and our current study is focused on one origin of the possible discrepancies.

* Corresponding author.

PII S0167-2789(97)00322-9

In general, the time interval τ_r between the consecutive intersections with the Poincaré surface is not constant. Usually τ_r as a function of the coordinates on this surface is bounded and continuous (as in the case of a Feigenbaum attractor), and there is no qualitative difference between the properties of the map and the flow. Moreover, in some situations it is possible to make the moments of intersections equidistant by shifting the secant surface and reparametrizing the time [1]; thus the flow becomes a suspension over the Poincaré mapping and their features coincide. An example is given by quasiperiodic motions, provided that the rotation numbers are not anomalously close to their rational approximants. On the other hand, it is known that discontinuities and singularities in τ_r may lead to a qualitative change of dynamical properties, like the birth of a continuous spectrum [2] or the onset of mixing [3,4]. In this contribution, we will address a situation where a saddle-point of the flow belongs to the closure of the attractor. Here τ_r is finite for those points at the Poincaré surface which do not lie on the intersection of this surface with the local stable manifold of the saddle. On the contrary, orbits which start from points close to this intersection slow down in the vicinity of the saddle; this results in a marked increase of τ_r. As a function of a coordinate (say, x) parametrizing some path along the Poincaré surface, the return time diverges at the intersection point x_0; this singularity is logarithmic ($\tau_r \sim -\log|x-x_0|$) for non-degenerate saddles and power-like ($\tau_r \sim |x-x_0|^{-\beta}$, $\beta > 0$) otherwise. Under these circumstances the averaged characteristics (like the Fourier spectra) computed from the map by a procedure which treats all the points uniformly and does not assign additional weights to the "neighborhood of singularity", can differ dramatically from those of the prototype flow. For instance, in the situation when the power spectrum of the flow is (singular) continuous, the return map may nevertheless have a discrete spectrum which is a signature of a qualitatively different type of dynamics. This situation was encountered in [5]; the objective of the current paper is to analyze the influence of the distribution of return times on the power spectrum.

Unbounded return times are inherent in continuous systems close to homoclinic and heteroclinic bifurcations. After a brief introduction to singular continuous spectra in Section 2, we proceed in Section 3 to the description of a particular dissipative flow whose attractor possesses the demanded properties, and develop in Section 4 a kind of an "improved" semi-discrete model which effectively accounts for the variations in return times. In Section 5 we reduce this model to self-similar symbolic sequences; the subsequent calculation of their spectral and correlation characteristics in Section 6 reproduces the respective features of the flow and demonstrates qualitative differences in comparison with the usual Poincaré mapping.

2. Singular continuous spectra in dynamics

Systems with singular continuous spectra constitute a kind of a bridge between regular behavior and chaotic dynamics. Unlike ordered systems, they do not preserve the complete information about the details of an initial state; nevertheless, unlike the chaotic systems, they still exhibit a kind of a vague memory about the distant past. The basic feature of this kind of dynamics is reflected in the name: the spectral measure is neither pure point (discrete) nor absolutely continuous with respect to the Lebesgue measure, but is singular continuous; its carrier is a dense Cantor set. The calculation of the power spectra for the observable ζ from the respective time series $\{\zeta_k\}$ through the familiar expression

$$S(\omega, l) = \frac{1}{l}\left\langle \left| \sum_{k=m}^{m-1+l} \zeta_k e^{i2\pi k\omega} \right|^2 \right\rangle \tag{1}$$

(the angular brackets denote averaging over the initial position m) fails to provide conventional results. With the increase of the sample length l, the partial sums $S(\omega, l)$ converge for a dense set of frequency values ω neither to constant values (which would correspond to an absolutely continuous spectrum), nor grow linearly with l (which

would hold for the discrete spectra). Usually they grow as $S(\omega, I) \sim I^{\gamma(\omega)}$ $(0< \gamma(\omega) <1)$, and one observes a "fractalization" of the spectral curve. Accordingly, estimation of the autocorrelation function

$$C(\tau) = \frac{\langle \zeta(t)\zeta(t+\tau)\rangle - \langle \zeta(t)\rangle^2}{\langle \zeta^2(t)\rangle - \langle \zeta(t)\rangle^2} \tag{2}$$

for such processes shows that the correlations neither ultimately decay for large τ, which would be the case for chaotic motion, nor display the infinite sequences of exact (or arbitrarily close) returns to unity, as for periodic (respectively, quasiperiodic) processes.

The autocorrelation function gives a reasonably reliable numerical tool for telling processes with singular continuous spectra from such with discrete or absolutely continuous ones. The necessary condition for the spectral measure to be absolutely continuous is the decay of correlations. On the other hand, the pure point component is absent if the value of the integrated correlation $C_{\rm int}(T) = (1/T)\int_0^T |C(\tau)|^2\,{\rm d}\tau$ vanishes for $T \to \infty$ [6]. Thus the numerical observation that the function $C(\tau)$ displays repetitive peaks of non-diminishing height over the longest computationally available values of τ whereas $C_{\rm int}$ decays (usually in a power-like way), provides reasons to conjecture that one has to do with a singular continuous spectrum. Keeping this criterion in mind, we will use the spectral vocabulary but make our judgments from the appearance of the respective autocorrelation functions.

3. The flow and its maps: affinity and mismatch

For our purpose we need a flow in which orbits on the attractor pass arbitrary close to the saddle point. This is the case for the Lorenz attractor [7] which contains the saddle point in its closure; however here already the Poincaré map delivers the fully chaotic dynamics [8] with positive Lyapunov exponent and continuous Fourier spectrum. A more appropriate example is provided by continuous dynamical systems at the accumulation point of the "homoclinic doublings" scenario. For such flows it has been recently demonstrated that their spectral properties can be qualitatively different from those of the induced return maps [5]. We will exploit this example to see in detail how the slowing down near the saddle results in the singularities of the power spectra.

As a starting point we take the following set of three ODEs [9]:

$$\dot{x} = \sigma(y-x) + \sigma D y(z-r), \qquad \dot{y} = rx - y - xz, \qquad \dot{z} = xy - bz, \tag{3}$$

which differ from the conventional Lorenz equations in their standard notation by the additional term proportional to the non-negative parameter D. The detailed description of the underlying hydro-mechanical problem, of the equations themselves and of the numerous bifurcation scenarios can be found elsewhere [5,9,10]; here we will only briefly cite the properties which are relevant for our current purpose. In the parameter region $D > (r-1)/r^2$ the trivial equilibrium $x = y = z = 0$ is a saddle with one-dimensional unstable manifold. Inside this region the increase of r eventually leads to the formation and subsequent destruction of homoclinic connections to the equilibrium; due to the symmetry $\{x, y\} \leftrightarrow \{-x, -y\}$ (inherited from the Lorenz equations), the homoclinic orbits always arrive in pairs. In the parameter domain $r - 1 - (\sigma + 1 - b)/\sigma < r^2 D < r - 1$ the positive eigenvalue λ_1, which locally characterizes the unstable direction, is smaller than the absolute value $|\lambda_2| = b$ of the leading (closest to zero) negative eigenvalue. This implies that unlike the Lorenz case, the destruction of the couple of homoclinic orbits does not create a chaotic set, but instead "glues" two stable mutually symmetrical closed orbits into a single one. In this way the length of the attracting trajectory in the phase space is doubled; notably, the period at the bifurcation point is infinite. Further increase of r leads through a bifurcation sequence in which symmetry-breakings of periodic orbits alternate with new homoclinic doublings (in systems with the Lorenz-like mirror symmetry each of these bifurcations is a codimension-1 event). The renormalization treatment of the reduced return mapping shows that

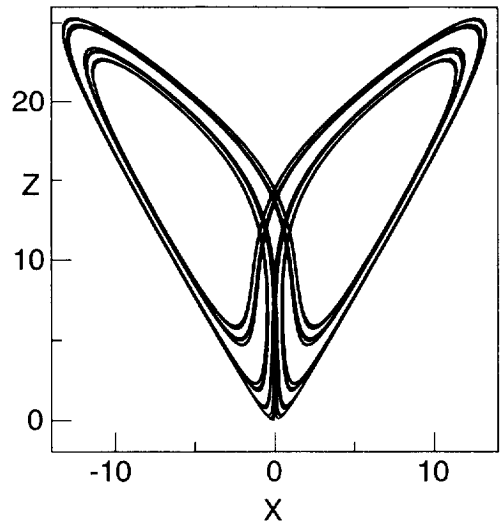

Fig. 1. Attractor for Eq. (3) at the accumulation point of homoclinic bifurcations ($\sigma = 10$; $b = 8/3$; $r = 15.82373667\ldots$; $D = 0.052634923\ldots$); The saddle point is located at the origin; the saddle index ν equals 2.0.

this sequence converges in a universal way [9,11]; the quantitative characteristics of the scenario (convergence rate, scaling properties of the resulting attracting set, etc.) depend only on the saddle index $\nu = |\lambda_2|/\lambda_1$ which uniquely determines the universality class.

The projection of this latter set is presented in Fig. 1; one notices both the reflection symmetry and the self-similar structure of the attractor. The unstable manifold Γ_u of (0, 0, 0) belongs to the attractor and provides a convenient way to characterize its scaling: starting from the outermost turn , the distance between the 2^n-th and 2^{n+1}-th turns of Γ_u decays as α^{-n}. The scaling factor α as a function of the saddle index ν monotonically decreases from $\alpha = \infty$ for $\nu = 1$ to $\alpha \to 1$ for $\nu = \infty$ (the latter case corresponds to vanishing of the eigenvalue λ_1 at the stability boundary of the equilibrium).

The geometry of the attractor admits the convenient symbolic coding. Let us assign the symbol R to each revolution of the orbit in the half-space $x > 0$ and the symbol L to the revolution in the half-space $x < 0$. At each homoclinic doubling the two mutually symmetric attracting orbits (whose codes turn into each other under the transformation $R \leftrightarrow L$) are glued together; thereby the code of the new attractor is simply the concatenation of the codes of its parents. This scenario runs through the steps $R \to RL \to RLLR \to RLLRLRRL\ldots$ and ends up with the symbolic object which is known as the Thue–Morse code [12,13] and is thoroughly studied in the theory of substitutions (see e.g. [14]). Among other features, this code (which can also be produced from a single symbol R by means of repetitive substitutions $R \to RL$, $L \to LR$) has a peculiar property: its spectral measure is singular continuous [15].

One would expect that the symbolic dynamics (as given by the Thue–Morse sequence) directly reflects the properties of the continuous system (3). Indeed, the estimates of power spectra computed from the finite series of the variables $x(t)$, $y(t)$ and $z(t)$ of the flow display no tendency to converge to smooth curves with the increase of the sample length [5]. Calculation of the autocorrelation function (Figs. 2(a) and (b)) demonstrates a series of moderate (distinctly lower than the unit value) peaks which, although becoming more and more seldom, preserve the same height (the rightmost peaks at these plots correspond to $\approx 2^{15}$ revolutions around the attractor). The integrated correlation function C_{int} decays within the same time interval by a factor of $\approx 10^3$ (Fig. 3). Thus, we have convincing numerical evidence that the criterion from preceding section is fulfilled: C_{int} decays whereas $C(\tau)$

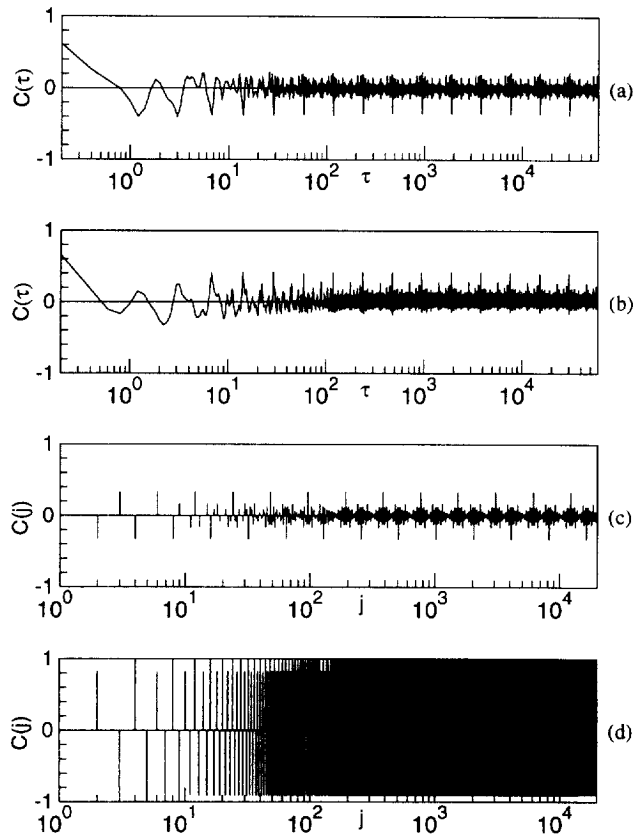

Fig. 2. Autocorrelation function in logarithmic timescale for the observables: (a) variable $x(t)$ for the attractor from Fig. 1; (b) variable $z(t)$ for the attractor from Fig. 1; (c) Thue–Morse sequence; (d) attracting orbit of f_z at m^*.

does not; accordingly, we may conjecture that the spectrum is singular continuous. (In fact, the analysis below implies that the discrete spectral component might be present as well, but its contribution seems to be exclusively small).

The autocorrelation function in logarithmic timescale for the variable $x(t)$ is plotted in Fig. 2(a); the whole structure is reminiscent of the correlation function for the Thue–Morse sequence (Fig. 2(c)). The latter can be computed with the help of the recurrent formulae $C(2\tau) = C(\tau)$, $C(2\tau+1) = -(C(\tau) + C(\tau+1))/2$; its largest peak values are $C(3\times 2^n) = -C(2^n) = 1/3, n = 0, 1, 2, 3\ldots$ [1] (A closer look at the two plots shows that this typical symmetry between the positive and negative peaks of $C(\tau)$ is absent for the continuous variable; accordingly, a finer symbolic description of the flow should yield the symbolic sequence with asymmetric autocorrelation function).

In studying the properties of the continuous system (3) the natural way is to reduce the dynamics to the return map; in presence of a stable foliation the map can be further reduced to a one-dimensional one. Should the surface of section be chosen transversely to the stable manifold of the saddle (in practice, fixing a small value of z is sufficient), this map will have a form

$$\xi_{i+1} = f_\xi(\xi_i) = (|\xi_i|^\nu - \mu)\ \mathrm{sign}(\xi_i) \tag{4}$$

[1] For the flows $C(\tau)$ is well defined for all τ; for a comparison with symbolic sequences and maps, one should choose in the continuous system times $t = n\tau_{\mathrm{av}}$ ($n = 1, 2, 3, \ldots$) where τ_{av} is the average duration of one loop (which for the attractor of Fig. 1 is 1.85465... in the dimensionless time units of (3)).

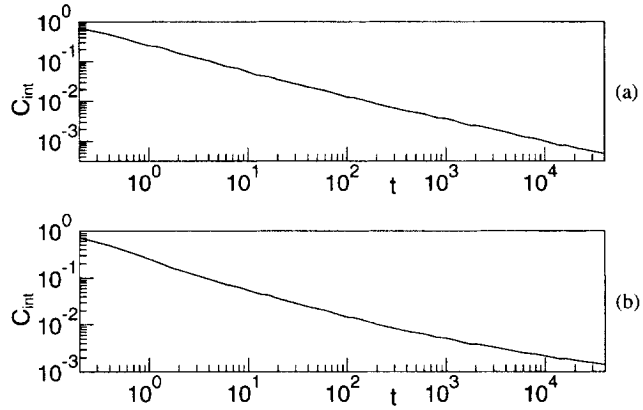

Fig. 3. Integrated autocorrelation in logarithmic timescale; the observables are (a) variable $x(t)$; (b) variable $z(t)$ from Eq. (3) for parameter values from Fig. 1.

up to the higher order terms in $\xi_i|\xi_i|^{\nu-1}$. Here the coordinate ξ is measured along the unstable manifold of the saddle; ν is the saddle index (unlike the Lorenz case, $\nu > 1$). The parameter μ characterizes the distance between the first return of the unstable manifold and the local stable manifold: $\mu = 0$ corresponds to the formation of a couple of simple (1-looped) homoclinic orbits. The two antisymmetric branches of the discontinuous map (4) correspond to the two components of the unstable manifold of the saddle-point of initial system. On assigning the symbol R (L) to iterations with positive (negative) ξ, one obtains a convenient coding; obviously, for the parameter value $\mu^*(\nu)$ which marks the accumulation of the homoclinic doublings, the symbolic code of the attractor is the Thue–Morse sequence. No wonder that the spectrum of the orbit of the map (4) at this parameter value also proves to be singular continuous.

The described way to construct the return map is by far not the only one; the Poincaré surface may be for instance any of cylinders whose axis passes through the saddle point and is perpendicular to the z-axis. Once again, the stable foliation reduces the dynamics to a one-dimensional map. If the map variable is chosen to be x or y or any combination thereof, then the map itself has the form of Eq. (4). However if one chooses the z-coordinate of the intersections, then (after proper rescaling, shift and truncation up to the terms of the order $O(|z_i|^\nu)$) the map takes the form

$$z_{i+1} = f_z(z_i) = \mu - |z_i|^\nu \tag{5}$$

(a similar expression is obtained for the return map of subsequent z-maxima as it was done in the initial paper of Lorenz [7]). Unlike Eq. (4), the map (5) is continuous and unimodal; on changing the parameter μ, instead of the sequence of homoclinic bifurcations the period-doubling scenario is encountered. Obviously, f_z is nothing else but the even counterpart of the odd f_ξ: one has $f_\xi(x) = f_z(x)\mathrm{sign}(x)$, and therefore, $|f_\xi^n(x)| = |f_z^n(x)|$ for each n. Consequently, there exists a one-to-one correspondence between the bifurcational parameter values in these two maps [11]: the symmetry-breakings of Eq. (4) correspond to period-doublings in Eq. (5), whereas the homoclinic bifurcations in Eq. (4) are matched by the points of superstability for the periodic orbits of the map (5). The convergence rate $\delta(\nu)$ of both scenarios depends on the saddle index ν; it increases monotonically from $\delta(1) = 2$ to $\delta(\infty) = 29.57\ldots$ [16]; obviously, for the case of quadratic singularity $\nu = 2$ it is given by the Feigenbaum constant: $\delta(2) = 4.669201\ldots$ The symbolic codings in the limiting points of both scenarios are the well-known symbolic itinerary of the period-doubling attractor [17] $\{P_j\} = RLRRRLRL\ldots$ and the Thue–Morse sequence $\{T_j\} = RLLRLRRL\ldots$ These codes are interrelated: if one starts with $T_1 = R$ and assigns the values of -1 and 1 to L and R respectively, the sequence $\{T_j\}$ can be obtained from $\{P_j\}$ by recursion:

$$T_{j+1} = \prod_{k=1}^{j}(-P_k) = -P_j T_j \tag{6}$$

However the dynamics on the period-doubling attractor which exists at $\mu = \mu^*(\nu)$, is not equivalent to its counterpart from Eq. (4): the values of the autocorrelation function $C(n)$ for the attractor of Eq. (5) approach 1 for even n (Fig. 2(d)); respectively, the power spectrum of z_j as well as the spectrum of the symbolic itinerary $\{P_j\}$ are both pure point.

Thus two one-dimensional reductions of the same two-dimensional Poincaré map prove to have attractors with qualitatively different dynamics. This seeming paradox is easily resolved when one recalls that the variables x and z have different symmetries with respect to the original flow. According to Eq. (6) the rule which yields the value of the nth element of the Thue–Morse sequence as a function of n is simply a skew product over the analogous rule for the period-doubling itinerary; it is known that a skew product over a dynamical system often possesses the richer spectral properties than the system itself [18]. Another discrepancy arises in relationship between the continuous variable $z(t)$ from (3) and its discretized version z_i from (5), as seen from the autocorrelation functions for the former (Fig. 2(b)) and for the latter (Fig. 2(d)). One notices series of persistent peaks in Fig. 2(b); although these are definitely lower than 1, the correlations do not ultimately decay. Combined with the apparent decay of the integrated function $C_{\mathrm{int}}(t)$ (Fig. 3(b)), this points to the singular continuous spectral component. This confirms that a "straightforward" discretization with the help of the return map fails to capture the basic feature of the dynamics, presenting it more ordered than it really is. As found in [5], the reason for this failure lies in the divergence of the return times near the saddle point, which remains unnoticed by the return map. Below we introduce the simplified model which incorporates the return times into this map, thus allowing us to see explicitly how the non-uniformity of the return times influences the power spectrum of the process.

4. Modeling non-equal return times

Our starting point is the continuous dependence $z(t)$ from Eq. (3) (as plotted in Fig. 4(a)); our aim is to obtain a map which adequately models the spectral properties of $z(t)$. The crosses mark the intersections of the orbit with the cylinder $x^2 + y^2 = 9$ (with $\mathrm{d}(x^2 + y^2)/\mathrm{d}t > 0$); the resulting sequence $\{z_i\}$ induces a mapping f_z. As seen from Fig. 4(a), the peaks are sharp and the valleys are broad (the lower the minimum, the broader the plateau around it). The system spends a noticeable time in the region of relatively small z, that is, near the saddle point where the "velocity" of the imaging point is much lower than elsewhere. It is therefore natural that characteristics (correlation functions, spectra etc.) averaged over time are strongly influenced by the contributions of the low-amplitude part of the orbit. One can hope to extract the necessary information from the points $\{z_i\}$. However, as we know, taking the mapping f_z as it is would be insufficient, since it does not take into account the differences between the durations of residence at different z_i's.

Let us couple the return map on the Poincaré surface to the temporal distribution of returns. Consider the discontinuous process $u(t)$ where $u(t)$ admits the constant value z_j (or ξ_j, if one models the variable $x(t)$) for the whole interval of time between the jth and $(j+1)$th intersections; it jumps to z_{j+1} (respectively, ξ_{j+1}) in the right endpoint of this interval (Fig. 4(b)). This construction in which the time is continuous and the observable variable is piecewise constant, is known under the name of "special flow" [18], and can be viewed as the map whose iterations are separated by non-equal time differences. Thus, the return times turn into the "residence durations".

Near the non-degenerate saddle point the return time has a logarithmic singularity; we model it by the function

$$\tau_{\mathrm{r}}(u) = A + B \log \frac{1}{|u|}, \tag{7}$$

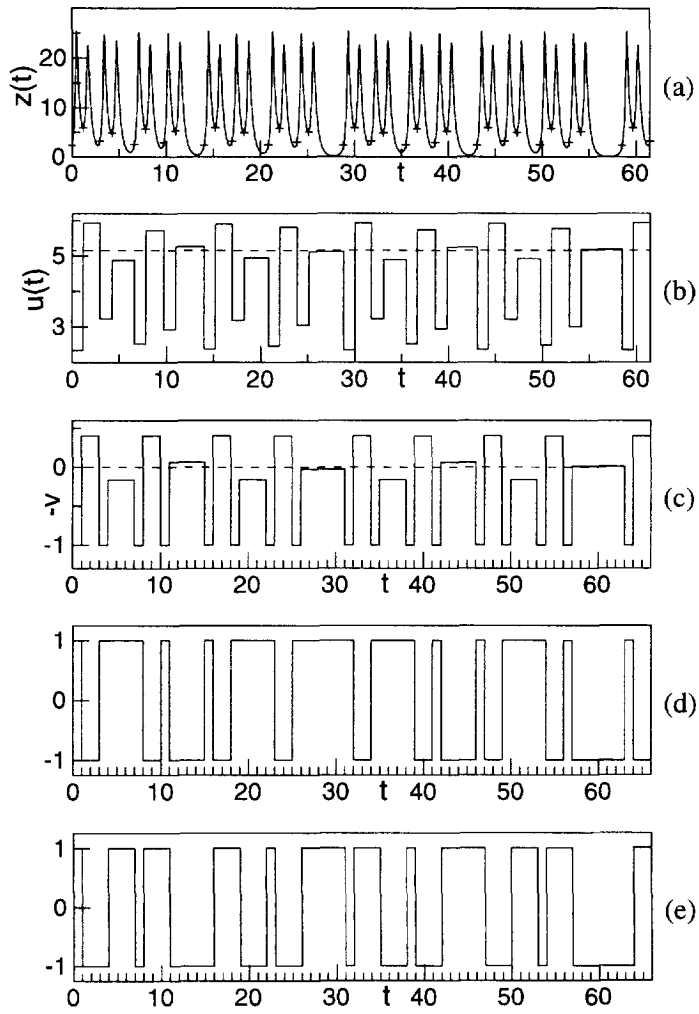

Fig. 4. Time dependencies corresponding to 34 orbit turns (residence durations in (c), (d) and (e) are given by (9)): (a) variable $z(t)$ (crosses denote intersections with Poincaré surface); (b) special flow $u(t)$ over the mapping induced by crosses in subplot (a); dashed line denotes the preimage of the extremum of z_j; (c) special flow over the variable v_n with $\alpha = 2.5$ and $\tau_0 = 0$ (as compared to $u(t)$, v is shifted and rescaled, and its sign is changed); (d) process reconstructed from the period-doubling code; (e) process reconstructed from the Thue–Morse sequence.

where the variable u stands both for ξ_i from (4) and z_i from (5). Here, the logarithmic term is responsible for the hovering near the saddle, and the u-independent term A gives roughly the time spent on the global (distant from the saddle) segment of the orbit loop. By itself, the knowledge of the coordinate dependence $\tau_r(u)$ does not yet provide the statistics of return times: this would also require the complete knowledge of the distribution of the values of u on the attractor. We approximate this distribution taking use of the scaling properties.

Both for the scenario of homoclinic doublings in (4) and for the period-doubling sequence in (5) the Feigenbaum–Cvitanović renormalization equation $g(u) = \alpha g(g(u/\alpha))$ [19] yields the universal function $g(u)$ which is discontinuous (piecewise increasing) in the former case and has extrema of order ν in the latter. Since Eq. (7) is logarithmic, presentation on logarithmic scale is especially illuminating (Fig. 5): one sees that the points on the attractor are

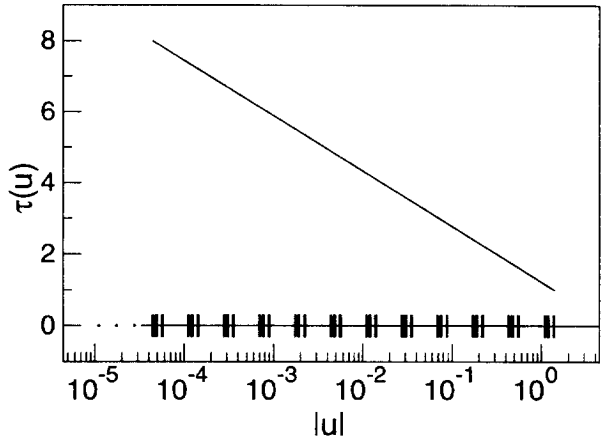

Fig. 5. Logarithmic coordinate dependence of residence durations $\tau(u)$ in the points of the attractor (points of the period-doubling attractor are marked along the abscissa).

grouped around the values $d_n = g^{2^n}(0) = \alpha^{-n} g(0)$, with the size of the nth "cluster" being of order $d_n/|\alpha|$. Take the sequence $\{u_i\}$ obtained from $u_0 = 0_+$ by iterating the function f_ξ or f_z. The nth iteration of the extremum lies in the $(j+1)$th cluster where $j(n)$ is the number of the first non-zero coefficient m_j in the binary expansion of n: $n = \sum_{j=0}^{\infty} m_j 2^j$ (thus, all odd iterations belong to the first cluster located at a distance of μ^* from the origin). In our further estimates we neglect the distances between the points within the same cluster. In other words, instead of the sequence $\{u_n\}$ we consider the values $v_n \equiv \mu^* |\alpha|^{-j(n)} \mathrm{sign}(u_n)$. For v_n the value of $\tau_r(v_n)$ equals

$$\tau_r(v_n) = \tau_r(\mu^* |\alpha|^{-j(n)}) = A - B \log \mu^* + B\, j(n) \log |\alpha|. \tag{8}$$

Apparently, this approximation should work better for larger values of $|\alpha|$, that is, in the range of not too large values of the saddle index ν.

Let the time be measured in units of $B \log |\alpha|$; in these units Eq. (8) can be rewritten as

$$\tau_r(v_n) = \frac{A - B \log(\mu^* |\alpha|)}{B \log |\alpha|} + 1 + j(n) \equiv \tau_0 + (1 + j(n)). \tag{9}$$

In this notation, τ_0 is the contribution of the global segment, and the bracketed term presents the logarithmic divergence of residence times on the attractor with geometric scaling: for all the odd values of n it equals 1, for the even values which are not multiples of 4, it equals 2, etc.

The mean residence duration under the law (9) is $\tau_0 + 2$; it corresponds in the original continuous system to the average duration of one turn of the trajectory on the attractor. Evolution of the "continuous" variable reconstructed in this way from the discrete sequence $\{v_n\}$ for the unimodal map (5) with ν=2 is plotted in Fig. 4(c). The autocorrelation function for this process (Fig. 6(a)) is qualitatively very similar to $C(\tau)$ computed for the original continuous variable $z(t)$ and plotted in Fig. 2(b).

5. Transformation of symbolic sequences

Insofar, we approximated the range of $z(t)$ by the set $\{\mu^* |\alpha|^{-j(n)}\}$ without any qualitative changes in the auto-correlations. A further simplification eliminates the coordinate values at all; we replace $u(t)$ in the special flow by $\mathrm{sign}(u)$. The process obtained in this way from the special flow over the period-doubling attractor is presented in

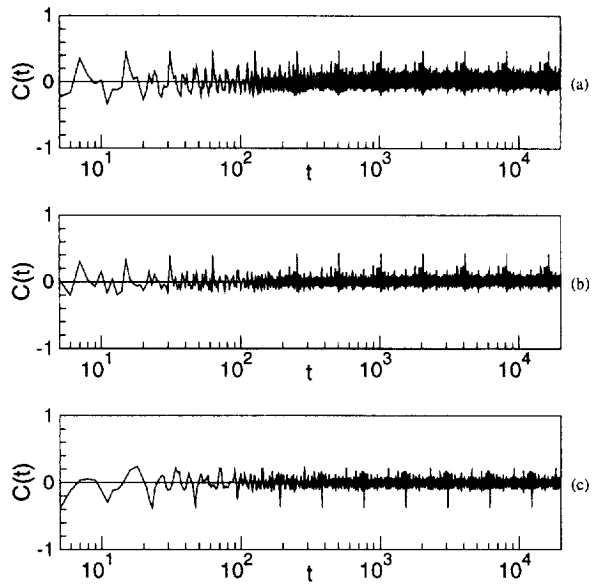

Fig. 6. Autocorrelation function in logarithmic timescale for the observables: (a) variable $v(t)$ from Fig. 4(c); (b) process reconstructed from period-doubling code (as in Fig. 4(d)); (c) process reconstructed from the Thue–Morse code (as in Fig. 4(e)).

Fig. 4(d); the analogous procedure applied to the special flow over the discontinuous map (4) yields the process shown in Fig. 4(e). The respective autocorrelation functions are plotted in Figs. 6(b) and (c); their likeness to the autocorrelation functions of the original continuous variables $z(t)$ and $x(t)$ is apparent. Noteworthy, the plot in Fig. 6(c) has lost the typical up–down symmetry of the autocorrelation function for Thue–Morse sequence.

The rough description with the help of sign(u) is in fact nothing else but coding with two symbols. Therefore, another way to view the results of this last simplification could be the following: Given the symbolic sequence, we prescribe the "residence duration" of the nth symbol by $\tau_r(n) = \tau_0 + (1 + j(n))$, and build in this way a kind of a special flow over the symbolic sequence. From this point of view, the plots in Figs. 4(d) and (e) present continuous-time processes reconstructed from the period-doubling code and the Thue–Morse sequence, respectively.

Now let us assume that τ_0 is a non-negative integer and go back from continuous time to symbolic sequences. For example, starting from the Thue–Morse sequence $\{T_j\} = R\,L\,L\,R\,L\,R\ldots$, taking $\tau_0 = 0$ and keeping in mind that $j(1) = j(3) = j(5) = 0$, $j(2) = j(6) = 1$, etc., we arrive at the sequence in which the second and the sixth symbol of $\{T_j\}$ are repeated twice, the fourth one is repeated three times, and so on: $R\,LL\;\;L\,RRR\,L\,RR\ldots$

From now on the object of our studies will be symbolic codes obtained by introducing the residence durations into $\{P_j\}$ and $\{T_j\}$. In fact, instead of the direct evaluation of these durations for each particular symbol, we will utilize the self-similarity of the codes. There are two equivalent methods to construct a self-similar symbolic sequence from an initial segment. One of them is to substitute recursively each letter of this segment by a prescribed sequence of symbols; in this way the sequence is "inflated" from inside. The other method is the concatenation: one deals with several sorts of symbolic "bricks" which are consecutively added to one another in the prescribed order; the result is treated as a new set of bricks, the procedure being repeated *ad infinitum*. During this process the "head" of the sequence (which is just the initial segment) remains unchanged whereas the "tail" grows and gets longer and longer.

Let us discuss briefly the first of these methods. At each step of the substitution (inflation) each symbol is substituted according to a specific rule. For both initial sequences these rules involve two letters: the period-doubling

code $\{P_j\}$ can be obtained from the initial symbol R by repeated substitutions $R \to RL$, $L \to RR$, and the Thue–Morse sequence evolves from the same R under the action of the symmetric substitution $R \to RL$, $L \to LR$. The inflation rules which take into account the distribution of residence durations, require four letters in both cases. For the code $\{\Pi_j\}$ obtained from $\{P_j\}$, the rule is

$$A \to ABC, \quad B \to AAD, \quad C \to D, \quad D \to C. \tag{10}$$

One should start with the symbol A; before assigning the numerical values to the letters, each A must be replaced by a chain of $\tau_0 + 1$ symbols R, each B should be identified with $\tau_0 + 1$ subsequent L's, each C becomes a single L and each D becomes a single R, respectively. The code $\{\Upsilon_j\}$ built over the Thue–Morse sequence is generated from $\Upsilon_1 = A$ by the inflation rule

$$A \to ABC, \quad B \to BAD, \quad C \to D, \quad D \to C \tag{11}$$

with the same condition for replacements before identifying the symbols with numbers. In each case, after m steps the sequence consists of $2^m - 1$ symbols. It is convenient to characterize the substitution with the help of its associated matrix [20,21]. Let our alphabet consist of k symbols $a_1, a_2, \ldots, a_k$. Take an arbitrary word in which all the letters are represented (this requirement excludes a risk of picking a word from the subset of alphabet which is substituted only through its own elements), and inflate it. The relation between the numbers of entries of each type $n_{a_1}, \ldots, n_{a_k}$ in the initial word and the respective numbers $n'_{a_1}, \ldots, n'_{a_k}$ for the transformed word, is

$$\begin{pmatrix} n'_{a_1} \\ \vdots \\ n'_{a_k} \end{pmatrix} = M \begin{pmatrix} n_{a_1} \\ \vdots \\ n_{a_k} \end{pmatrix} \tag{12}$$

and M is called the associated matrix of the substitution rule. In case of the period-doubling code this matrix is

$$\begin{pmatrix} 1 & 2 \\ 1 & 0 \end{pmatrix},$$

and for the Thue–Morse sequence it is

$$\begin{pmatrix} 1 & 1 \\ 1 & 1 \end{pmatrix}.$$

Noteworthy, the ordering of symbols in the substitution finds no reflection in M; only the overall numbers of entries of each type count. According to the conjecture of Bombieri and Taylor [20], spectral properties of the symbolic code are determined by the location of eigenvalues of the associated matrix for its substitution rule: a discrete component must be present, if the so-called Pisot–Vijayaraghavan (PV) condition is satisfied. This condition requires that strictly one eigenvalue is larger than one whereas the rest of the eigenvalues lies within the unit circle. Already the Thue–Morse code provides an important exception to this rule: although the PV condition is fulfilled (the eigenvalues are 2 and 0), the spectrum, instead of being discrete, is singular continuous.

The associated matrix for the substitution (10) is

$$\begin{pmatrix} 1 & 2 & 0 & 0 \\ 1 & 0 & 0 & 0 \\ 1 & 0 & 0 & 1 \\ 0 & 1 & 1 & 0 \end{pmatrix} \tag{13}$$

with the eigenvalues $(2, 1, -1, -1)$; the respective matrix for (11) is

$$\begin{pmatrix} 1 & 1 & 0 & 0 \\ 1 & 1 & 0 & 0 \\ 1 & 0 & 0 & 1 \\ 0 & 1 & 1 & 0 \end{pmatrix}, \tag{14}$$

its eigenvalues being $(2, 1, 0, -1)$. In neither of these two cases is the PV condition fulfilled: along with the eigenvalue 2 one has to do with several marginal eigenvalues belonging to the unit circle.

To get an idea of the spectral properties of $\{\Pi_j\}$ and $\{\Upsilon_j\}$ one can further exploit the associated matrices (13) and (14), similarly to the technique used in [21] for studies of quasiperiodically ordered short and long bonds on the line. To our mind, however, the other recursive way to build the same symbolic sequences looks more appropriate for this purpose: to produce them with the help of the concatenation rules.

Concatenation of two strings is simply writing the second after the end of the first. In the following, the very last letter of a string Ψ will be denoted as ψ_{E}, and the string Ψ *without* this last symbol will be denoted as ψ_{B} (thus $\Psi = \psi_{\mathrm{B}}\psi_{\mathrm{E}}$). For a binary string, the overbar will denote the "mirror image": given the string A, the string $\overline{A}$ defines the string in which each 1 (or, in our context, R) of A is changed to -1 (L) and vice versa.

The concatenation rule for building the Thue–Morse sequence has been already demonstrated above while describing the scenario of homoclinic doublings. The string $\Psi^{(n+1)}$ obtained from $\Psi^{(1)} = R$ after n concatenations consists of 2^n symbols, and is produced by appending to $\Psi^{(n)}$ its opposite:

$$\Psi^{(n+1)} = \Psi^{(n)}\overline{\Psi^{(n)}}. \tag{15}$$

The analogous rule for the period-doubling code involves two steps. At first, $\Psi^{(n)}$ is concatenated with itself: $\Psi^{(n)} \to \Psi^{(n)}\Psi^{(n)}$, and then the very last letter of the resulting word is converted to the opposite one: $R \leftrightarrow L$.

$$\Psi^{(n+1)} = \Psi^{(n)}\psi_{\mathrm{B}}^{(n)}\overline{\psi_{\mathrm{E}}^{(n)}}. \tag{16}$$

Evaluation of the respective spectral sums $S(\omega, l)$ shows that the power spectrum is discrete for Eq. (16) and singular continuous for Eq. (15) (see e.g. [5]).

In order to take account for the residence durations, rules (15) and (16) require only a slight modification: in each case the last letter of the concatenated word should be repeated. This yields

$$\Psi^{(n+1)} = \Psi^{(n)}\overline{\Psi^{(n)}\psi_{\mathrm{E}}^{(n)}} \tag{17}$$

for the code $\{\Upsilon_j\}$, and

$$\Psi^{(n+1)} = \Psi^{(n)}\psi_{\mathrm{B}}^{(n)}\overline{\psi_{\mathrm{E}}^{(n)}\psi_{\mathrm{E}}^{(n)}} \tag{18}$$

for the code $\{\Pi_j\}$, respectively. Besides, the initial condition should be reformulated: now $\Psi^{(1)}$ is a string of $\tau_0 + 1$ symbols R. Obviously, in both cases after n concatenations the resulting object consists of $l_n = (\tau_0 + 2)2^n - 1$ letters and is identical with the string obtained by applying n respective substitutions to the same initial word.

6. Spectral characteristics of symbolic codes

Let us proceed with the estimation of the spectral sums $S(\omega, l_n)$. We begin with the code $\{\Upsilon_j\}$ derived from the Thue–Morse sequence. Consider $Z_n(\omega) = \sum_{k=1}^{l_n} \Upsilon_k e^{2\pi i\omega k}$. From Eq. (17) follows:

$$Z_{n+1}(\omega) = Z_n(\omega)(1 - e^{2\pi i\omega l_n}) + \Upsilon_{l_{n+1}} e^{2\pi i\omega l_{n+1}}, \tag{19}$$

and further,

$$|Z_{n+1}(\omega)|^2 = 2|Z_n(\omega)|^2(1-\cos 2\pi\omega l_n) + 1 + \Upsilon_{l_{n+1}}(Z_n(\omega)(1-e^{2\pi i\omega l_n})e^{-2\pi i\omega l_{n+1}} + Z_n^*(\omega)(1-e^{-2\pi i\omega l_n})e^{2\pi i\omega l_{n+1}}). \tag{20}$$

In the following we consider only such values of ω for which the spectral sums $S(\omega, l_n) = l_n^{-1}|Z_n(\omega)|^2$ at least do not decay for large n, i.e. for which $|Z_n(\omega)|$ grows not slower than $\sqrt{l_n}$. For these values of ω one can neglect on the right-hand side of Eq. (20) the terms proportional to $\Upsilon_{l_{n+1}}$ (recall that $|\Upsilon_j| = 1$) and the summand 1. For large n this leaves us with

$$S(\omega, l_{n+1}) \approx S(\omega, l_n)(1-\cos 2\pi\omega l_n). \tag{21}$$

We will treat it as an exact recurrent relation; combined with the relationship between l_{n+1} and l_n, this provides us with the two-dimensional mapping

$$S_{n+1} = S_n(1-\cos 2\pi\theta_n), \tag{22}$$

$$\theta_{n+1} = (2\theta_n + \omega) \bmod 1 \tag{23}$$

whose orbit starts from initial conditions $S_1 = 1, \theta_0 = (\tau_0+1)\omega$.

The map (22) and (23) is a skew product: the dynamics of the second variable does not depend on the first one. We are interested in the evolution of S_n; its mean growth (or decay) rate is determined by the geometric average $\varrho = \langle 1-\cos 2\pi\theta_n\rangle$ along the respective orbit of (23): $S_n \sim l_n^{\bar\lambda}$ where $\bar\lambda = \log\varrho/\log 2$. Generally speaking, (23) is a chaotic map with uniform invariant density, a variant of the Bernoulli shift [18], but for each given ω we are interested in the particular orbit starting at θ_0. In terms of the variable $(\theta+\omega)$ the map acquires the familiar Bernoulli form; from this point of view, changing ω in Eq. (23) is equivalent to changing initial value in the Bernoulli map. If ω is rational, the respective orbit is either periodic or eventually periodic (in the latter case it becomes periodic after a certain initial segment). For the fixed period p ($p = 1, 2, 3, \ldots$) the corresponding values of ω are given by

$$\omega = \frac{l}{(\tau_0+2)2^m(2^p-1)}, \tag{24}$$

where m is an arbitrary non-negative integer and l is an odd integer between 0 and $(\tau_0+2)2^m(2^p-1)$. For $m \neq 1$ the orbit is eventually periodic: the actual periodic orbit located at

$$\theta = \frac{l}{2^p-1}\left(1-\frac{1}{2^m(\tau_0+2)}\right) \bmod 1 \tag{25}$$

is reached at the $(m-1)$th iteration of (23).

As an example, we present in Table 1 the values of $\bar\lambda$ for several periodic orbits of (23) and compare them to the analogous values evaluated from the sequence $\{\Upsilon_j\}$. In the latter case the estimates to $\bar\lambda$ are given by the expression:

$$\lambda_l(\omega) = (p\log 2)^{-1}\log\frac{1+2^{1-l}\sum_{k=1}^{2^l-1}(2^l-1-j)C(k)\cos 2\pi\omega k}{1+2^{1+p-l}\sum_{k=1}^{2^{l-p}-1}(2^{l-p}-1-j)C(k)\cos 2\pi\omega k}, \tag{26}$$

where $C(k)$ is the value of the autocorrelation function for $\{\Upsilon_j\}$. According to numerics, the quite satisfactory convergence of λ_l is attained already for moderate (≥ 12) l's.

The remarkably good correspondence between the positive growth rates provides an a-posteriori justification for our reduction of (20) to (21). Moreover, the last row of the upper half of the table and the penultimate row of the lower half display this correspondence even in case of the moderate ($-1/2 < \lambda < 0$) decay of the spectral sums.

Table 1
Growth rates of the spectral sums for the sequence $\{\Upsilon_j\}$

τ_0	p	ω	ϱ	$\bar{\lambda}$	λ_{12}	λ_{13}	λ_{14}	λ_{15}
0	1	3/8	$1+2^{-1/2}$	0.77155	0.77389	0.77246	0.77051	0.76632
0	1	5/16	1.38268	0.46747	0.47425	0.47118	0.47420	0.47088
0	1	1/4	1	0	0.00596	0.00639	0.00414	−0.00024
0	2	1/12	1.36602	0.44998	0.46043	0.45512	0.45339	0.45256
0	2	5/12	0.36602	−1.44998	−0.78587	−0.81555	−0.83187	−0.85719
0	2	5/24	0.75882	−0.39817	−0.34811	−0.35401	−0.38569	−0.38767
1	1	1/3	3/2	0.58496	0.58509	0.58579	0.58760	0.58416
1	2	1/9	1.26604	0.34033	0.34297	0.34105	0.33910	0.34032
1	3	2/7	1.10809	0.14807	0.15206	0.15412	0.15128	0.15044
1	3	9/28	0.91566	−0.12711	−0.11465	−0.11612	−0.11653	−0.12446
1	3	8/21	0.10203	−1.09761	−0.88704	−0.91565	−0.92706	−0.93559

Only the faster decay (cf. the last row in the table), as expected, cannot be properly described with the help of relations (22) and (23). Consequently, we conjecture that some part of the spectral measure is concentrated on the countable set of the rational values of (ω) with $\bar{\lambda}(\omega) \geq 0$. For all the periodic and eventually periodic orbits with $p > 1$ and nearly all fixed and eventually fixed points with $p = 1$ (the exceptions will be separately discussed below) the value of $\bar{\lambda}$ is distinctly lower than 1; accordingly, the spectral sums grow with n slower than linearly, and the respective values of ω belong to the singular continuous spectral component.

For the irrational values of ω the corresponding orbit of (23) is chaotic. The distribution of the invariant measure on the interval (0, 1) is uniform, and for the generic value of ω the rate λ can be computed simply by averaging the ratio $\log(1-\cos 2\pi\theta)/\log 2$ on this interval; this yields $\bar{\lambda} = -1/2 - 1/4\pi \approx -0.579$ and ensures the rapid decay of the respective spectral sums. However, the Bernoulli map includes also the continuum of trajectories which stay anomalously close to the rational values of ω. Let us pick out from this continuum the trajectories which repeatedly hover near the periodic orbits with positive $\bar{\lambda}$. An iteration of the Bernoulli map is simply a unit shift along the binary representation of the number. One should cut out the very long segments from the binary representations of ω for different periodic orbits with positive $\bar{\lambda}$, and concatenate them into the infinite binary sequence. Obviously, the leftmost segment of the sequence is of no importance, and the orbit can be started arbitrarily close to any given point. This procedure provides a dense non-denumerable set of irrational (if we reject the periodic concatenations) values of ω with $\bar{\lambda}(\omega) > 0$; roughly speaking, this is just the set which carries the spectral measure.

The peculiar circumstance is associated with the value $\omega = \frac{1}{2}$: this is a fixed point of (23) for any integer τ_0, and the growth rate for it equals 1: $S(1/2, l_n) \propto l_n$ which produces the δ-peak in the power spectrum. Hence the spectrum should be a mixture of the discrete and the singular continuous component. The visual absence of the former, as implied by the apparent decay of the integrated autocorrelation function $C_{\mathrm{int}}(t)$ in Fig. 3, can be attributed to the weakness of the contribution of the discrete part; this contribution must be especially small, should τ_0 be non-integer (this aspect is further discussed below in the final paragraph of this section).

Now let us turn to the sequence $\{\Pi_j\}$ obtained from the period-doubling code. In this case we have

$$Z_{n+1}(\omega) = Z_n(\omega)(1 + \mathrm{e}^{2\pi \mathrm{i}\omega l_n}) - 2\Pi_{l_n}\mathrm{e}^{2\pi \mathrm{i}\omega(l_{n+1}-1)} + \Pi_{l_{n+1}}\mathrm{e}^{2\pi \mathrm{i}\omega l_{n+1}}, \tag{27}$$

and using the same assumptions as above, the recursion for the spectral sums S_n is derived:

$$S_{n+1} = S_n(1 + \cos 2\pi\theta_n), \tag{28}$$

$$\theta_{n+1} = (2\theta_n + \omega) \bmod 1. \tag{29}$$

Table 2
Growth rates of the spectral sums for the sequence $\{\Pi_j\}$

τ_0	p	ω	ϱ	$\bar{\lambda}$
0	1	3/8	$1-2^{-1/2}$	−1.77155
0	1	5/16	0.61731	−0.69591
0	1	1/4	1	0
0	2	1/12	0.36602	−1.44984
0	2	5/12	1.36602	0.44984
0	2	5/24	0.24118	−2.05181
1	1	1/3	1/2	−1
1	2	1/9	0.26604	−1.91026
1	3	2/7	0.25157	−1.99090
1	3	9/28	0.21360	−2.22696
1	3	8/21	0.10203	0.47403

The map (29) coincides with (23); consequently, the same expression (24) provides us with the complete list of the values of ω corresponding to periodic and eventually periodic orbits. On the other hand, the difference between (22) and (28) means that for each of these orbits the growth/decay rate for the spectral sums of $\{\Pi_j\}$, in general, is not the same as in the case of $\{\Upsilon_j\}$ (Table 2). Thus, for the orbit with period 1 the decay for $\{\Pi_j\}$ always implies growth for $\{\Upsilon_j\}$ and vice versa, since the respective values of ϱ are related by $\varrho(\Pi) + \varrho(\Upsilon) = 2$. On the whole, however, we obtain qualitatively the same picture: decay of spectral sums for almost all irrational values of ω and part of the rationals, as opposed to the growth (with $\bar{\lambda} < 1$) of these sums for the rest of the rationals and the remaining dense subset of the irrationals.

On the first sight, it may seem that in this situation the discrete component might be absent: although $\theta = 1/2$ remains the fixed point of the map (29), the respective growth rate vanishes identically. However, there are countably many eventually periodic orbits of (29) with period 1 whose growth rate λ is arbitrarily close to 1. The last iteration on the transient, before reaching the periodic orbit, passes very close to $\theta = 1/2$; respectively, the spectral sum is multiplied by a tiny factor and nearly vanishes after this iteration. The subsequent fast growth begins from the very small starting position; for this reason, to observe the presence of the discrete component, one needs really long samples.

The above discussion refers to the local properties of the spectral measure. The global description should characterize the set which carries this measure as a whole; this would inevitably require the multifractal analysis, because the generalized dimensions D_q of this set are apparently different (thus, its capacity D_0 equals 1, since the values of ω with positive $\bar{\lambda}$ are dense). The complete picture is delivered by the singularity spectrum $f(\alpha)$ (for the applications of thermodynamical formalism to singular continuous spectra see, e.g. [5,22]); here we will limit ourselves to the numerical estimates for the correlation dimension D_2 of the fractal component of the spectrum. It has been recently proved that in systems with purely singular continuous spectra the correlation dimension of the spectral measure predetermines the decay rate of the integrated autocorrelation function [23,24]: $C_{\text{int}}(T) \sim T^{-D_2}$. Our situation is more complicated: the above analysis predicts the presence of discrete component in the power spectra of both $\{\Pi_j\}$ and $\{\Upsilon_j\}$, which means that $C_{\text{int}}(T)$ should not decay to zero but will instead tend to some finite positive value. At present we are not aware of rigorous mathematical relations between the dimensions of the spectral measure and the properties of integrated correlations for the case of mixed power spectra. For this reason we will use the empirical extrapolation from the pure singular case, employed in [25] for the mixed spectrum of the kicked Harpers model. Let the contribution of the discrete spectral component be $C_{\text{int}}(\infty) \equiv A \ \ (A > 0)$; we assume that the rate of convergence to A is a reasonably good approximation to D_2: $C_{\text{int}}(T) - A \sim T^{-D_2}$ and estimate the values of A and D_2 by numerical fitting of the $C_{\text{int}}(T)$ dependencies.

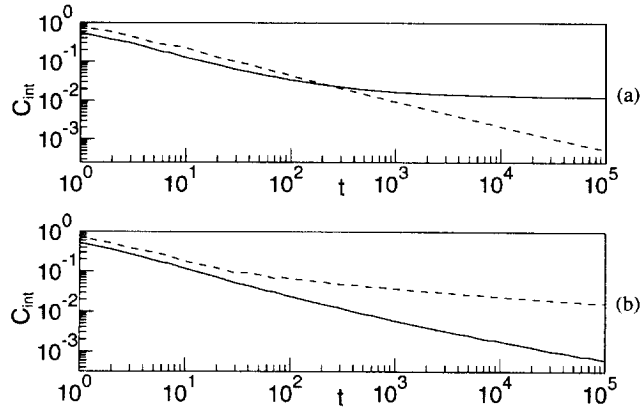

Fig. 7. Integrated autocorrelation in logarithmic timescale for the observables: (a) symbolic sequence $\{\Upsilon_j\}$: $\tau_0 = 0$ (solid line) and $\tau_0 = 3$ (dashed line); (b) symbolic sequence $\{\Pi_j\}$: $\tau_0 = 0$ (solid line) and $\tau_0 = 3$ (dashed line).

Let us take as a reference point the prototype symbolic sequences $\{P_j\}$ and $\{T_j\}$. The spectral measure of the period-doubling code is pure-point, hence for the former $D_2 = 0$. The value of D_2 for the spectral measure of the Thue–Morse sequence equals $3 - \log(1 + \sqrt{17})/\log 2 = 0.64298\ldots$ [26].

Fitting the data on C_{int} from Fig. 3, obtained from the integration of the initial continuous system (3), we come to the values $A \approx 1.9 \times 10^{-4}$, $D_2 \approx 0.63$ for the variable $x(t)$ and $A \approx 8.1 \times 10^{-4}$, $D_2 \approx 0.56$ for the variable $z(t)$.

Coming now to the corresponding data for $\{\Upsilon_j\}$ (Fig. 7(a)), we observe that the weight of the discrete component in the power spectrum is strongly dependent on τ_0: the best-fitted value of A may be as large as 1.2×10^{-2} for $\tau_0 = 0$ and as small as 9.1×10^{-5} for $\tau_0 = 3$. However, this seems to exert little (if at all) influence on the slope D_2: for the checked values $0 \leq \tau_0 \leq 6$ the estimates on D_2 lie within the range (0.64–0.68). Thus we see that, both for the flow and its discrete models, even on the quantitative level the fractal component of the spectral measure, as inherited from the Thue–Morse sequence, does not change its global properties in spite of the action of the logarithmic divergence in the return (residence) times.

The results for $\{\Pi_j\}$ are much less conclusive. Again, the intensity of the discrete spectral component A is strongly influenced by the value of τ_0 (Fig. 7(b)). However, here also the slope D_2 exhibits large fluctuations depending on τ_0: from $D_2 \approx 0.58$ for $\tau_0 = 0$ to $D_2 \approx 0.36$ for $\tau_0 = 3$. In the Thue–Morse case, introduction of the residence durations has enforced the onset of a weak discrete spectral component upon the singular continuous background; here, on the contrary, the very existence of the singular continuous part of the spectrum is due to these unequal residence times. For this reason, the properties of the fractal component seem to be very sensitive to the details of the pattern of residence durations.

The final remark concerns the origin of the mixed character of the spectrum. On the first sight, the presence of the discrete spectral component follows from the provision that the time of global reinjection τ_0 should be integer. One can hardly expect that in a generic continuous system the mean time of global reinjection would be commensurate with the average time of hovering near the saddle point. In fact, this provision is formally needed neither for the inflation rules (10) and (11) nor for the concatenations (17) and (18). The associated substitution matrices are τ_0-independent. The only place where it really matters is the substitution of the "original" symbols R and L into the inflated codes. Should we allow the process to be described in terms of four (and not two) symbols, τ_0 can easily be rendered non-integer. Then the partial spectral sums (1) turn into the Fourier integrals, and the assumption that they do not decay when the sample length grows, leads to the very same skew products: (22) and (23) for the process obtained from the Thue–Morse sequence and (28) and (29) for the suspension over the period-doubling code. Under

irrational τ_0 all the periodic and eventually periodic orbits correspond to irrational values of ω; for this reason, say, in the Thue–Morse case, $\theta = 1/2$ would not be a fixed point. However, admission of non-integer values of τ_0 does not provide an ultimate remedy, since for any of these values the eventual fixed points can be found arbitrarily close to 1/2; respectively, the growth rate $\overline{\lambda}$ can be made arbitrarily close to 1, the corresponding spectral component being indistinguishable from the delta-function. Noteworthy, linear growth starts only after hitting the fixed point, and the preceding transient may well be long. Each new iteration of the skew product is equivalent to the doubling of the sample length; this means that the integer values of τ_0 simply make the discrete component of the power spectrum better resolvable in short samples.

7. Discussion

Self-similar properties of the prototype Thue–Morse and period-doubling symbolic sequences play the crucial role in our derivation of substitution and concatenation rules for the processes with logarithmic singularities of return times. Although inherent for the scenario of "homoclinic doublings", these properties are absent in the general case when the flow does not possess the Lorenz-like mirror symmetry, and the road to chaos through the homoclinic bifurcations in the parameter space follows one of the multitude of the possible routes [10,27,28]. All of these routes are associated with unbounded times of return on the secant surface (and hence, for all of them the flow is not equivalent to the Poincaré map), but only a countable subset can be characterized through self-similarities. In the latter case one can build up the corresponding concatenation rules and examine with their help the laws which govern the growth of the spectral sums; in the more general case a kind of a statistical approach could be more helpful.

The same methods can be applied to other situations in which the origin of the singular continuous spectral component is related to singularities of return times: e.g. in Hamiltonian flows on a 2-torus with saddle points and irrational rotation numbers [4,29], or in the hydrodynamical variant of the problem: the forced steady flow of a viscous fluid on a doubly periodic domain in presence of a mean drift [30].

In this paper we have demonstrated that particular mechanisms for the appearance of multifractal power spectrum in continuous dissipative systems can be adequately described by means of symbolic dynamics. In fact, the role played in the above analysis by the dissipative character of the flow is restricted to the effective reduction of dynamics to one-dimensional maps; the proper account of the logarithmic divergence of return times seems to be more important, and we expect that similar considerations should work also in the context of low-dimensional conservative systems. An open question remains, whether an adequate symbolic description is possible for a general continuous flow. As soon as such description is obtained, the well-developed theory of spectral properties of symbolic sequences [14] can serve as a basis for understanding dynamical systems at the border between order and chaos.

Acknowledgements

We are grateful to C. Godrèche, K.M. Khanin, J.-M. Luck, A. Politi and W.-M. Zheng for fruitful discussions and useful suggestions. The research of MZ was supported by the MPG grant.

References

[1] H. Broer, F. Takens, Arch. Rational Mech. Anal. 124 (1993) 13.
[2] J. von Neumann, Ann. Math. 33 (1932) 587.
[3] A.V. Kochergin, Math. Notes 19 (1976) 277.
[4] Ya.G. Sinai, K.M. Khanin, Func. Anal. Appl. 26 (1992) 155.

[5] A.S. Pikovsky, M.A. Zaks, U.Feudel, J. Kurths, Phys. Rev. E 52 (1995) 285.
[6] N. Wiener, J. Math. Phys. 6 (1926) 145.
[7] E.N. Lorenz, J. Atmos. Sci. 20 (1963) 130.
[8] V.S. Afraimovich, V.V. Bykov, L.P. Shilnikov, Sov. Phys. Doklady 22 (1977) 253.
[9] D.V. Lyubimov, M.A. Zaks, Physica D 9 (1983) 52.
[10] D.V. Lyubimov, A.S. Pikovsky, M.A. Zaks, in: S.P. Novikov (Ed.), Mathematical Physics Review, vol. 8, Gordon and Breach, Chur, 1989, pp. 221–292.
[11] A. Arneodo, P. Coullet, C. Tresser, Phys. Lett. A 81 (1981) 197.
[12] A. Thue, Norske vid. Selsk. Skr. I. Mat. Nat. Kl. Christiania 7 (1906) 1.
[13] M. Morse, Trans. AMS. 22 (1921) 84.
[14] M. Queffélec, Substitution Dynamical Systems – Spectral Analysis, Lecture Notes in Mathematics, vol. 1294, Springer, Berlin, 1987.
[15] K. Mahler, J. Math. Phys. 6 (1926) 158.
[16] J.-P. Eckmann, H. Epstein, Comm. Math. Phys. 128 (1990) 427.
[17] P. Collet, J.-P. Eckmann, Iterated Maps on the Interval as Dynamical System, Birkhäuser, Basel, 1980.
[18] I.P. Cornfeld, S.V. Fomin, Ya.G. Sinai, Ergodic Theory, Springer, New York, 1982.
[19] M.J. Feigenbaum, J. Stat. Phys. 19 (1978) 25.
[20] E. Bombieri, J. Taylor, J. Phys., Colloq. C3 47 (1986) C3-19.
[21] S. Aubry, C. Godrèche, J.M. Luck, J. Stat. Phys. 51 (1988) 1033.
[22] C. Godrèche, J.M. Luck, J. Phys. A 23 (1990) 3769–3797.
[23] R. Ketzmerick, G. Petschel, T. Geisel, Phys. Rev. Lett. 69 (1992) 695–698.
[24] M. Holschneider, Comm. Math. Phys. 160 (1994) 457–473.
[25] R. Artuso, D. Belluzzo, C. Casati, Europhys. Lett. 25 (1994) 181.
[26] M.A. Zaks, A.S. Pikovsky, J. Kurths, J. Stat. Phys. 88 (1997) 1387.
[27] J.-M. Gambaudo, I. Procaccia, S. Thomae, C. Tresser, Phys. Rev. Lett. 57 (1986) 925.
[28] I. Procaccia, S. Thomae, C. Tresser, Phys. Rev. A 35 (1987) 1884.
[29] A.V. Kochergin, Math. Sbornik 96 (1975) 471.
[30] M.A. Zaks, A.S. Pikovsky, J. Kurths, Phys. Rev. Lett. 77 (1996) 4338.